JOURNAL OF INTEGRAL EQUATIONS
AND APPLICATIONS
Volume 21, Number 3, Fall 2009

THE METHOD OF FUNDAMENTAL SOLUTIONS FOR DETECTION OF CAVITIES IN EIT

D. BORMAN, D. B. INGHAM, B. T. JOHANSSON AND D. LESNIC

Communicated by Simon Chandler-Wilde, Ivan Graham and J. Trevelyan

JIEA: A special Issue for the UKBIM6 Meeting

ABSTRACT. In this paper, the method of fundamental solutions (MFS) is used to solve numerically an inverse problem which consists of finding an unknown cavity within a region of interest based on given boundary Cauchy data. A range of examples are used to demonstrate that this technique is very effective at locating cavities in both two- and three-dimensional geometries for exact input data. The MFS is then developed to include a regularisation parameter that enables cavities to be located accurately and stably even for noisy input data.

1. Introduction. Electrical Impedance Tomography (EIT) is a technique in which an image of the permittivity, or conductivity, of the interior of an object such as the human body is inferred from surface measurements of electrical quantities. Practically, this can be achieved by attaching conducting electrodes to the boundary of a person or object and applying small alternating currents to some or all of the electrodes. The resulting voltages are measured and the process repeated for numerous different configurations of applied current. The electrical potential produced across the object containing the cavity depends on the particular location and the electrical properties of the cavity and, as such, it should be possible to use boundary measurements of the voltage to detect and locate such cavities [Hanke and Bruhl 2003, Holder 2005]. This allows an approximate image of the spatial distribution of the electrical conductivity within the object to be constructed [Borcea 2002].

Keywords and phrases. Electrical impedance tomography, inverse problems, method of fundamental solutions.
Received by the editors on November 9, 2007, and in revised form on June 13, 2008.
DOI:10.1216/JIE-2009-21-3-381

As a non-invasive technique, EIT can be of particular benefit when it is used for medical imaging. The process uses no ionising radiation and therefore it is possible to use the procedure for continuous monitoring. The problem of recovering the conductivity information is a nonlinear and ill-posed inverse problem. As such, one of the current drawbacks to the technique is a low spatial resolution [Boone 2006].

We consider the inverse problem of determining an unknown conductor D compactly contained in a bounded domain $\Omega \subset \mathbb{R}^d$, $d = 2, 3$, i.e. $D \subset \Omega$, entering the Laplace equation

$$\bigtriangledown^2 u = 0 \qquad \text{in } \Omega \setminus \overline{D}, \quad \text{with } u|_{\partial D} = 0, \tag{1}$$

from the knowledge of a single Cauchy pair of nontrivial data $(u, \partial_n u)$ on the boundary $\partial\Omega$ of Ω, where $\boldsymbol{n}$ is the outward unit normal to $\partial\Omega$ and u is the electrical potential. This type of mathematical model appears in many applications of electric field sensing [Smith 1996, Smith et al. 1998]. In EIT, the homogeneous condition $u|_{\partial D} = 0$ means that the inclusion D is a perfect conductor, i.e. of infinite conductivity.

It has been shown in earlier work [Borman et al. 2007] that the MFS procedure is a technique that accurately approximates the direct problem solution in both two- and three-dimensions and it will be developed in this paper for solving numerically the inverse problem of identifying the unknown cavity D entering in (1).

2. Mathematical Formulation. Let Ω and D be bounded domains with smooth boundaries such that $\overline{D} \subset \Omega$, and $\Omega \setminus D$ is connected. Let $f \in H^{1/2}(\partial\Omega)$ be the given applied voltage potential, not identically zero. Then f generates the electric field $E = - \bigtriangledown u$, where the electric potential u satisfies the following Dirichlet problem:

$$\bigtriangledown^2 u = 0 \qquad \text{in} \quad \Omega \setminus \overline{D}, \tag{2}$$

$$u = 0 \qquad \text{on} \quad \partial D, \tag{3}$$

$$u = f \qquad \text{on} \quad \partial\Omega. \tag{4}$$

Note that if the inclusion D is an insulator, i.e. of zero conductivity, then condition (3) should be replaced by $\partial_n u = 0$ on ∂D.

When D is known, it is well-known that the Dirichlet problem for the Laplace equation, as given by equations (2) - (4), has a unique solution

$u \in H^1(\Omega)$. Then we can define a nonlinear operator F_f, which maps from the set of admissible subdomains D to the data space of Neumann values in $H^{-1/2}(\partial\Omega)$ as follows:

$$F_f(D) := \partial_n u|_{\partial\Omega} = \mathrm{g} \in H^{-1/2}(\partial\Omega). \tag{5}$$

Then the inverse problem under consideration consists of extracting some information about the domain D from the data $F_f(D)$. As opposed to the direct problem, the inverse problem is nonlinear and ill-posed. The issue of uniqueness, i.e. the identifiability of an unknown perfectly conducting curve ∂D from the Cauchy data $(f \not\equiv 0, \mathrm{g})$ on $\partial\Omega$, can be found in [Kress 2004]. The uniqueness can also be established for the identifiability of an unknown perfectly insulated curve ∂D from the Cauchy data $(f \not\equiv \mathit{constant}, \mathrm{g})$ on $\partial\Omega$ with $\int_{\partial\Omega} \mathrm{g}\, ds = 0$, [Haddar and Kress 2005]. Stability estimates were obtained in [Alessandrini and Rondi 2001].

Since the response operator F_f is a highly nonlinear function of the domain D, extracting useful information from the measurements is a difficult computational problem. If one is interested only in the location of D, then one can employ efficiently the plane or sphere search method for tracking the position of a two- or three-dimensional cavity D, respectively, as described in [Kim et al. 2002]. On the other hand, if the location, shape and size of the obstacle D are all of interest then one can use iterative schemes which require the solution of many forward problems for each change of geometry and position of D, see e.g. [Duraiswami et al. 1997]. These authors used the Boundary Element Method (BEM) as a direct solver. It is the purpose of this paper to use instead the MFS due to its advantages over the BEM that stem mostly from the fact that the method is meshless and only the boundary of the domain of the problem under consideration needs to be 'discretised' (as a set of collocation points). This completely avoids any integral evaluation and makes no significant difference in coding between the two- and the three-dimensional cases [Burgess and Mahajerin 1984, Fairweather and Karageorghis 1998].

3. The Method of Fundamental Solutions (MFS). The MFS is a member of a class of boundary-type techniques that involve computations being undertaken with respect to points on the boundary of the region of interest. As such, they do not involve interior points of the

region of interest, which is useful in many real world engineering applications. Like the BEM, the MFS is an effective technique for solving linear elliptic partial differential equations with constant coefficients for which a fundamental solution is available in explicit form, such as the Laplace, biharmonic and Helmholtz equations. It is a form of indirect boundary integral equation method and a technique that uses boundary collocation or boundary fitting [Johnston and Fairweather 1984]. Based on density results for linear elliptic partial differential equations [Bogomolny 1985, Golberg and Chen, 1998], in the MFS we seek an approximation to the solution of the Laplace equation (1) as a linear combination of fundamental solutions, namely,

$$u(\boldsymbol{x}) \approx U_N(\boldsymbol{x}) = \sum_{j=1}^{N} C_j G_d(\boldsymbol{x}, \mathbf{y}_j), \qquad \boldsymbol{x} \in \overline{\Omega} \setminus D, \tag{6}$$

where G_d is a fundamental solution of the Laplace equation in $\mathbb{R}^d$ given by

$$G_d(\boldsymbol{x}, \xi) = \begin{cases} -\ln|\boldsymbol{x} - \boldsymbol{\xi}|, & \text{if} \quad d = 2, \\ \dfrac{1}{|\boldsymbol{x} - \boldsymbol{\xi}|}, & \text{if} \quad d = 3, \end{cases} \tag{7}$$

and the distinct singularities $(\mathbf{y}_j)_{j=\overline{1,N}}$ are located in $D \cup (\mathbb{R}^d \setminus \bar{\Omega})$. The following lemma [Alves and Martins, 2006] gives the linear independence and denseness results of the MFS based on the approximation (6).

Lemma 1. (i) *The set of functions* $\{\mathrm{G}_d(., \mathrm{y}_j)\}_{\overline{y=1,N}} : \overline{\Omega \setminus \mathrm{D}} \to \mathbb{R}$ *is linearly dependent.*

(ii) *Let* $\mathrm{D}_1 \subset \mathrm{D} \subset \Omega \subset \mathrm{D}_2 \subset \mathbb{R}^2$ *be two domains with regular boundaries* $\partial\mathrm{D}_1$ *and* $\partial\mathrm{D}_2$*. Then the set*

$$span\{\mathrm{G}_2(., \mathrm{y})|_{\partial\Omega}\,; \qquad \mathrm{y} \in \mathrm{D}_1 \cup \partial\mathrm{D}_2\} + \mathbb{R}$$

is dense in $\mathrm{L}^2(\partial\Omega)$*.*

In the first instance, we adopt the simpler version of the MFS, usually called the charge simulation method [Golberg and Chen 1998], in

which part of the singularities are known at fixed positions on an artificial boundary located outside $\overline{\Omega}$. The price to pay for not allowing the singularities to move in an adaptive and optimal way is that the location of the fixed artificial boundary has to be dealt with heuristically [Balakrishnan and Ramachandran 2000], although [Bogomolny 1985] suggested that theoretically the locations of singularities can be restricted to any surface embracing $\overline{\Omega}$. The remaining singularities are located in D and they are moving with the unknown object D throughout the iterative process described below.

In the direct problem given by equations (2) - (4), in which D is known, the unknown coefficients $(C_j)_{j=\overline{1,N}}$ in equation (6) are determined by imposing the boundary conditions (3) and (4). However, in the inverse problem (IP), given by equations (2) - (5), D is unknown. Let us consider a star shaped cavity D (with respect to the origin) whose boundary admits the polar (if $d = 2$), or the spherical (if $d = 3$) parameterizations

$$r = r(\theta), \qquad 0 < \theta \leq 2\pi, \tag{8}$$

or,

$$r = r(\Psi, \theta), \qquad 0 < \psi \leq \pi, \quad 0 < \theta \leq 2\pi, \tag{9}$$

respectively. Without reducing the generality of the problem we may assume that Ω is the unit circle (if $d = 2$), or the unit sphere (if $d = 3$).

For simplicity, let us consider the two-dimensional case. Based on expression (8), the boundary of D is pointified by

$$r_i = r(\theta_i), \qquad i - \overline{1, M}, \tag{10}$$

where

$$\theta_i = 2\pi i/M, \qquad i = \overline{1, M}.$$

Then the coefficients $(C_j)_{j=\overline{1,N}}$ and the radii $(r_i)_{i=\overline{1,M}}$ can be determined by imposing the boundary conditions (3) - (5) in a nonlinear least-squares sense which recasts into minimising the function

$$S(\mathbf{C}, \mathbf{r}) := \|U_N - f\|^2_{H^{1/2}(\partial\Omega)} + \|\partial_n U_N - g\|^2_{H^{-1/2}(\partial\Omega)} + \|U_N\|^2_{L^2(\partial D)}. \tag{11}$$

A few remarks about this function are worth mentioning at this stage:

(i) In the discretised version of (11), for technical computational reasons, we consider all the norms in L^2.

(ii) The constraints $0 < r_i < 1,\ i = \overline{1, M}$, are imposed during the iterative procedure by adjustment at each iteration ($\partial\Omega$ is the unit circle).

(iii) The current flux Neumann data (5) comes from practical measurements which are inherently contaminated with noisy errors and therefore,we replace g in (11) by g^ϵ, where

$$\|\mathrm{g}^\epsilon - \mathrm{g}\|_{L^2(\partial\Omega)} \leq \epsilon. \tag{12}$$

Based on the above remarks, it is natural to propose minimising the modified discretised objective cost function

$$S(\mathbf{C}, \mathbf{r}) := \sum_{i=1}^{M} [U_N(\boldsymbol{x}_i) - f(\boldsymbol{x}_i)]^2 + \sum_{i=1}^{M} [\partial_n U_N(\boldsymbol{x}_i) - g^\epsilon(\boldsymbol{x}_i)]^2 + \sum_{i=M+1}^{2M} [U_N(\boldsymbol{x}_i)]^2, \tag{13}$$

where

$$\boldsymbol{x}_i = (\cos(\theta_i), \sin(\theta_i)), \qquad i = \overline{1, M}, \tag{14}$$

are boundary collocation points uniformly distributed on $\partial\Omega = \partial B_2(0, 1)$, and

$$\boldsymbol{x}_{i+M} = (r_i \cos(\theta_i), r_i \sin(\theta_i)), \qquad i = \overline{1, M}, \tag{15}$$

are boundary collocation points on ∂D. Essentially, we have M collocation points taken on the outer boundary $\partial\Omega$ and M on the inner boundary ∂D of the cavity. It remains to specify the position of the singularities $(\mathbf{y}_j)_{j=\overline{1,N}}$ in $D \cup (\mathbb{R}^2 \setminus \overline{\Omega})$. These are taken as

$$\mathbf{y}_j = (R_{ext} \cos(\tilde{\theta}_j), R_{ext} \sin(\tilde{\theta}_j)), \qquad j = \overline{1, N_1}, \tag{16}$$

$$\mathbf{y}_{j+N_1} = \left(\frac{r_j}{s} \cos(\tilde{\theta}_j), \frac{r_j}{s} \sin(\tilde{\theta}_j)\right), \qquad j = \overline{1, M}, \tag{17}$$

where $s > 1, R_{ext} > 1, \tilde{\theta}_j = 2\pi j / N_1$ and $N = N_1 + M$.

Typically, the values of R_{ext} and s are taken as 2, meaning N_1 singularities are located at a radii twice that of the outer boundary and M singularities are located at a radii half that of the internal boundary.

In equation (13), U_N is given by (6) from which the normal derivative can be calculated as

$$\partial_n U_N(\boldsymbol{x}) = \sum_{j=1}^{N} C_j \partial_{n(x)} G_d(\boldsymbol{x}, \mathbf{y}_j), \qquad \boldsymbol{x} \in \partial\Omega, \tag{18}$$

where from (7)

$$\partial_{n(x)} G_d(\boldsymbol{x}, \boldsymbol{\xi}) = \begin{cases} -\frac{(\boldsymbol{x}-\boldsymbol{\xi})\cdot\boldsymbol{n}}{|\boldsymbol{x}-\boldsymbol{\xi}|^2}, & \text{if } d = 2, \\ -\frac{(\boldsymbol{x}-\boldsymbol{\xi})\cdot\boldsymbol{n}}{|\boldsymbol{x}-\boldsymbol{\xi}|^3}, & \text{if } d = 3\,. \end{cases} \tag{19}$$

The minimisation of the objective function (13) is performed computationally using the NAG routine E04FCF, which is a comprehensive algorithm for finding an unconstrained minimum of a sum of squares of m nonlinear functions in n variables, where no derivatives need to be provided by the user as they are calculated internally by the routine using forward finite differences.

The approach assumes that the cavity is star shaped and defined by M radii and the centre located at the origin, meaning that this will provide M unknowns to be found during the minimisation. In addition, the MFS procedure requires the vector of coefficients $\boldsymbol{C}$ to be found during the minimisation, i.e. the number of additional unknowns will be $N = M + N_1$. Therefore, the total number of unknowns to be found becomes $M + N = 2M + N_1$. The least squares minimisation (13) provides $3M$ equations. Since the number of equations should be greater or equal to the number of unknowns then this requires $3M = 2M + N_1$, or $M = N_1$.

An important point to finally note is that the gradient of the function (13) can be calculated analytically. In section 4 we will take $N_1 = M$ and this means we have $3M$ unknowns and $3M$ equations, hence $\theta_j = \tilde{\theta}_j$ for $j = \overline{1, M}$. We can then re-write (13) explicitly in two-dimensions as

$$
\begin{aligned}
(20)\quad S(\boldsymbol{C},\boldsymbol{r}) := \sum_{i=1}^{M}\Bigg[& \frac{1}{2}\sum_{j=1}^{M} C_j \ln\left[1+R_{ext}^2-2R_{ext}\cos(\theta_i-\theta_j)\right] \\
& + \frac{1}{2}\sum_{j=M+1}^{2M} C_j \ln\left[1+\left(\frac{r_{j-M}}{s}\right)^2-\frac{2r_{j-M}}{s}\cos(\theta_i-\theta_{j-M})\right] \\
& \qquad - f(\cos(\theta_i),\sin(\theta_i))\Bigg]^2 \\
& + \sum_{i=M+1}^{2M}\Bigg[\sum_{j=1}^{M} C_j \frac{1-R_{ext}\cos(\theta_{i-M}-\theta_j)}{1+R_{ext}^2-2R_{ext}\cos(\theta_{i-M}-\theta_j)} \\
& + \sum_{j=M+1}^{2M} C_j \frac{1-\frac{r_{j-M}}{s}\cos(\theta_{i-M}-\theta_{j-M})}{1+\left(\frac{r_{j-M}}{s}\right)^2-\frac{2r_{j-M}}{s}\cos(\theta_{i-M}-\theta_{j-M})} \\
& \qquad - g^{\epsilon}(\cos(\theta_{i-M}),\sin(\theta_{i-M}))\Bigg]^2 \\
& + \sum_{i=2M+1}^{3M}\Bigg[\frac{1}{2}\sum_{j=1}^{M} C_j \ln[r_{i-2M}^2+R_{ext}^2-2r_{i-2M}R_{ext}\cos(\theta_{i-2M}-\theta_j)] \\
& + \frac{1}{2}\sum_{j=M+1}^{2M} C_j \ln\Bigg[r_{i-2M}^2+\left(\frac{r_{j-M}}{s}\right)^2 \\
& \qquad -\frac{2r_{i-2M}r_{j-M}}{s}\cos(\theta_{i-2M}-\theta_{j-M})\Bigg]\Bigg]^2,
\end{aligned}
$$

and then differentiate this expression with respect to C_k for $k=\overline{1,2M}$ and r_l for $l=\overline{1,M}$ to explicitly find the gradient $\nabla S(\boldsymbol{C},\boldsymbol{r})$.

3.1. *Discussion on previous MFS approaches.* In principle, the MFS described above for the solution of the inverse cavity problem is in fact a discretised version of the hybrid method of Kirsch and Kress [Kirsch and Kress 1986, 1987], compare [Colton and Kress 1998, 2006, Serranho 2007] previously described, however this was described only in the inverse acoustic scattering context. Similar MFS approaches have been recently developed for the numerical solution of the inverse cavity problem in elasticity [Alves and Martins 2009] and Stokes flows

[Martins and Silvestre 2008]. For the inverse cavity problem in steady heat conduction or electrostatics, i.e. for the Laplace equation (2), previous MFS approaches [Alves and Martins 2006] assume either a Fourier parametrisation of the boundary ∂D, or seek the unknown cavity as the zero level set of the MFS solution. In our approach described above we do not employ these techniques.

4. Numerical Results and Discussion.

4.1 Example 1. As a first example, we consider a simple two-dimensional detection of an unknown circular cavity $D = B_2(0, r_0)$ of radius $r_0 \in (0, 1)$ within the unit circle $\Omega = B_2(0, 1)$. We take $f = -\ln(r_0)$ on $\partial\Omega$ in (4) and then the direct problem given by equations (2) - (4), when $D = B_2(0, r_0)$ is known, has the unique solution

$$u(r, \theta) = \ln(r/r_0), \qquad r_0 \leq r \leq 1, \qquad 0 < \theta \leq 2\pi\,. \tag{21}$$

The initial guess for the vector $\boldsymbol{C}$ is $\mathbf{0.1}$ in all Examples 1-3. The initial guess for the cavity is taken as a circle located at the origin with radius 0.5 unless explicitly stated otherwise. This is typical for problems of this structure where a cavity is being located in the unit circle. Numerical results are presented for $R_{ext} = s = 2$ and $M = N_1 = 30$. We have found that for $M > N_1$ the convergence became faster, but if $M = N_1$ increases over 30 convergence problems with the NAG routine E04FCF were observed.

4.1.1. *No noise.* The cavity to be identified was located at the origin of radius $r_0 = 0.7$ and consider first the case when there is no noise added to the measured data (5), i.e. $\epsilon = 0$. Figure 1(a) shows the results obtained from the minimisation routine following a series of 200 iterations. It can be clearly seen that the routine locates the cavity with a high accuracy as the result exactly overlays the analytical desired cavity. Figure 1(b) shows the objective function (20) as a function of the number of iterations. From this figure it can be seen that for the first 100 iterations the solution remains almost at the initial guess after which it drops for the next 100 iterations and finally it drops to zero after about a total of 200 iterations. Equally satisfactory results were obtained when we searched for cavities of radii 0.8, 0.6, 0.4, 0.3 or 0.2.

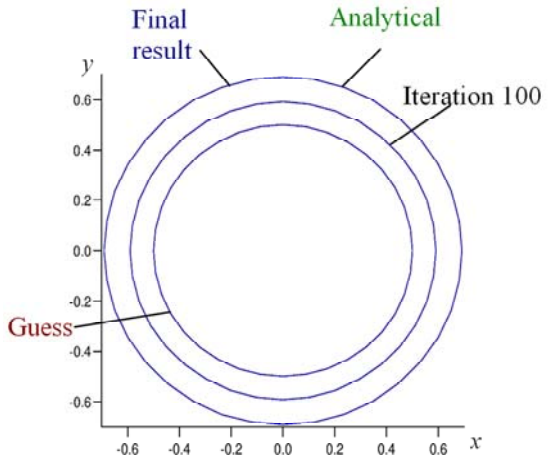

Figure 1a: The output from the minimisation routine for Example 1 when searching for a circular cavity located at the origin of radius $r_0 = 0.7$.

Small errors in the final location accuracy arise when cavities of size 0.1 or less are attempted to be retrieved.

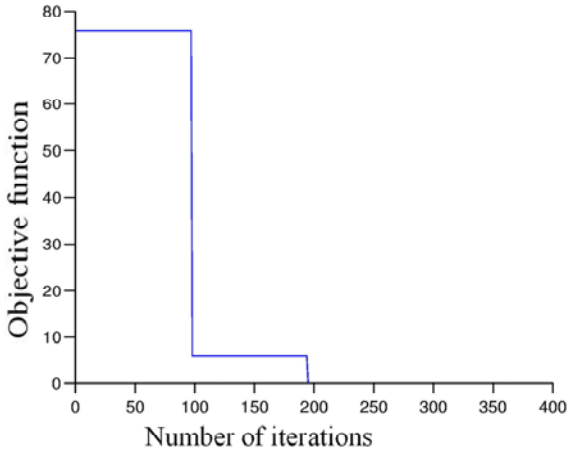

Figure 1b: The objective function as a function of the number of iterations.

4.1.2. *Adding noise to the boundary data.* To simulate real measured data, random noise is introduced into the Neumann boundary data g

as g^ϵ given by

$$g^\epsilon(x_i) = 1 + \epsilon_i, \qquad i = \overline{1, M}, \tag{22}$$

where ϵ_i are Gaussian random variables with mean zero and standard deviation $\sigma = p\% =$ percentage of noise, generated using the NAG routine G05DDF. As expected, since the inverse cavity problem is ill-posed and no regularisation was included in the objective least-squares functional (13), the addition of noise to the data (22) gave inaccuracies and instabilities into the numerically obtained results even when very small amounts of noise were used.

4.1.3. *Summary of the results obtained.* The results obtained for Example 1 show that the technique employed is capable of detecting circular cavities of various radii positioned at the origin of a unit circle when an initial guess of a circle of radius 0.5 located at the origin is used. Using this procedure enables circles as small as radii 0.2 to be located accurately when no noise is introduced in the input data. When noise is added into the normal derivative term (22), the routine fails to locate the cavity regardless of the mesh size employed. It is anticipated that the inclusion of a regularisation term into the objective function (13) will improve the stability of the results.

4.1.4. *Incorporating a regularising term.* Regularisation is necessary in order to obtain a stable solution when noisy data g^ϵ is used in (13). In this case we modify the functional S given by equation (13) by adding to it the regularisation term

$$T(\lambda_1, \lambda_2, \lambda_3, \boldsymbol{C}, \boldsymbol{r}) = \lambda_1 \sum_{j=1}^{2M} C_j^2 + \lambda_2 \sum_{j=1}^{M} r_j^2 + \lambda_3 \sum_{j=2}^{M} (r_j - r_{j-1})^2, \tag{23}$$

where $\lambda_1, \lambda_2, \lambda_3 \geq 0$ are regularisation parameters. The second term imposes the continuity of the boundary ∂D, whilst the third term imposes the smoothness C^1 of the boundary ∂D. If the boundary ∂D is *a priori* known to be of class C^2 then (23) could include an extra term $\lambda_4 \sum_{j=3}^{M} (r_j - 2r_{j-1} + r_{j-2})^2$. It should be noted that one can take

$\lambda_2 = 0$ whenever $\lambda_3 > 0$ since the first-order regularisation includes the zeroth-order regularisation. In the following numerical experiments we will only discuss, for simplicity, numerical results obtained using the zeroth-order regularisation, i.e. $\lambda_3 = 0$ in (23).

4.1.5. *Results with regularisation.* In the first instance we investigate results when $\lambda_3 = 0$ and $\lambda_1 = \lambda_2$, for the simplicity of having only one regularisation parameter to specify. Then, the regularisation term (23) becomes

$$T(\lambda_1, \boldsymbol{C}, \boldsymbol{r}) = \lambda_1 \left\{ \sum_{j=1}^{2M} C_j^2 + \sum_{j=1}^{M} r_j^2 \right\}. \tag{24}$$

The circular cavity to be identified was located at the origin of radius $r_0 = 0.4$. Figure 2(a) shows how the routine successfully locates the cavity as the final result exactly overlays the analytical solution when no noise is used. Figure 2(b) shows the objective function when no noise is used and it can be observed that the function reaches approximately zero after 200 iterations.

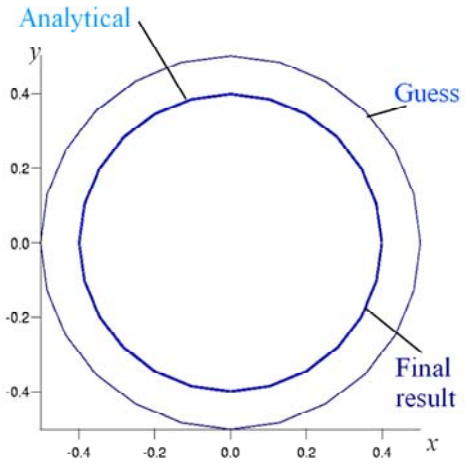

Figure 2a: The output from the minimisation routine after the final iteration for Example 1 when searching for a circular cavity located at the origin of radius $r_0 = 0.4$ with the addition of no noise.

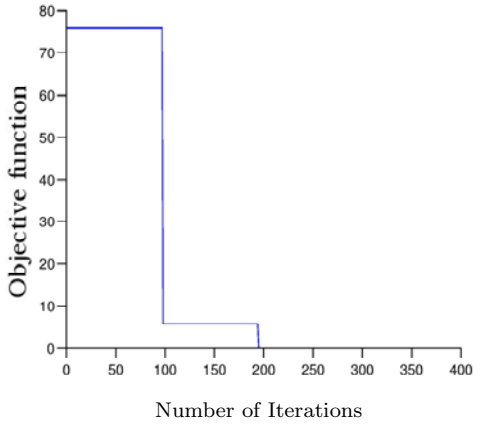

Figure 2b: The objective function, as a function of the number of iterations, for Example 1 when searching for a circular cavity located at the origin of radius $r_0 = 0.4$ with the addition of no noise.

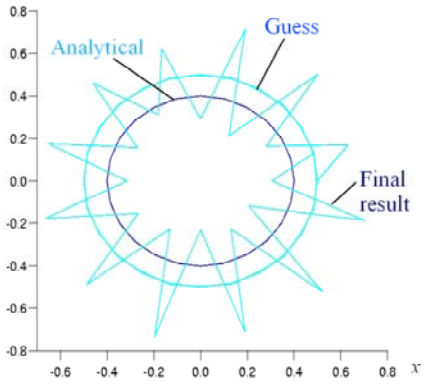

Figure 2c: The output from the minimisation routine after the final iteration for Example 1 when searching for a circular cavity located at the origin of radius $r_0 = 0.4$ with the addition of 1% noise.

A meaningless result is obtained from the results of the minimisation routine when 1% noise is included in the data (22) and no regularisation is used, i.e. $\lambda_1 = 0$ in (24), see Figure 2(c). It can be observed in Figure 2(d) that, consistent with the cavity not being located, the objective function fails to minimise. The results for 5% noise were observed

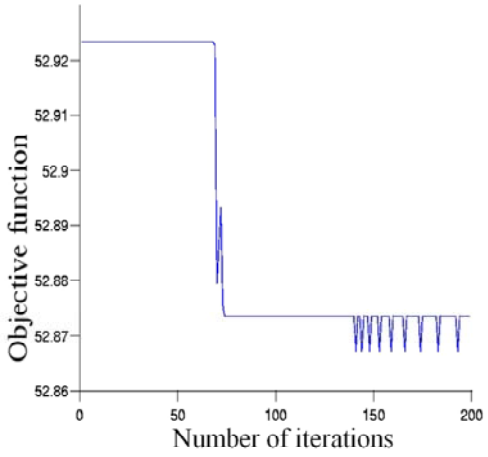

Figure 2d: The objective function, as a function of the number of iterations, for Example 1 when searching for a circular cavity located at the origin of radius $r_0 = 0.4$ with the addition of 1% noise.

to have very similar characteristics to those of 1% noise. Figure 2(c) further illustrates the ill-posedness of the inverse problem and that classical ordinary least-squares methods produce unstable numerical solutions.

Figure 3 shows the objective function obtained when the regularisation parameter $\lambda_1 = 0.05$ is used in (24) for 1%, 3% and 5% noise. In comparison to Figure 2(d), it can be observed that the results are significantly improved with the objective functions approaching zero in each case. The smaller the amount of noise, the faster the objective function approaches zero.

These objective function results are reflected in the accuracy of the cavity location. In Figure 4(a) it can be clearly observed that the cavity is located very accurately when 1% noise is employed and in Figure 4(b) the $r_0 = 0.4$ radius cavity is located with reasonable accuracy when 5% noise is used.

4.1.6. *Searching for a range of cavity sizes.* We have observed that the MFS successfully solves problems with noisy data by including a regularisation parameter for the case of locating cavities of radius 0.4, located at the origin. It is advantageous to validate the technique by

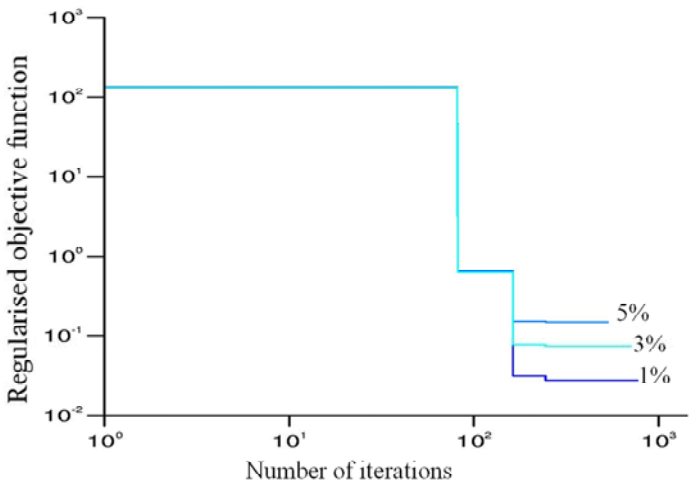

Figure 3: The regularised objective function for Example 1, as a function of the number of iterations, with $\lambda_1 = 0.05$ for various amounts of noise 1%, 3% and 5%, when searching for a cavity located at the origin of radius $r_0 = 0.4$.

attempting to locate cavities of different sizes.

Cavities of various sizes located at the origin with radii 0.2, 0.6, 0.8 were investigated. In the first instance, the value of the regularisation parameter is kept the same as in the previous case as this helps to indicate if the parameter is robust for a range of cavity sizes. Figure 4 (a) shows the results obtained when a regularisation parameter of $\lambda_1 = 0.05$ is used for 1% noise and Figure 4 (b) shows the equivalent result for 5% noise. It can be observed that the results demonstrate very high accuracy for the 1% noise. For 5% noise the larger cavities are located with high accuracy. However, we observed a progressive deterioration in accuracy as the size of the cavities diminished.

The robustness of the technique with the constant regularisation parameter are very encouraging for the MFS approach as they show that when using the same value of the regularisation parameter then multiple sizes of cavities can be located with a high level of accuracy, even when up to 5% noise is employed. Further values of λ_1 were investigated without any significant improvement in the results obtained for the 5% case. The successful implementation of the MFS technique for

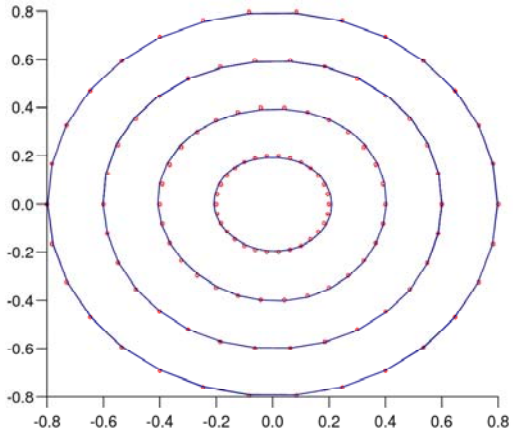

Figure 4a: The output of the regularised minimisation routine for Example 1 with $\lambda_1 = 0.05$ after the final iteration when searching for circular cavities of radii $r \in \{0.2, 0.4, 0.6, 0.8\}$ for 1% noise. The dots represent the analytical targets whilst the continuous lines represent the numerical values retrieved.

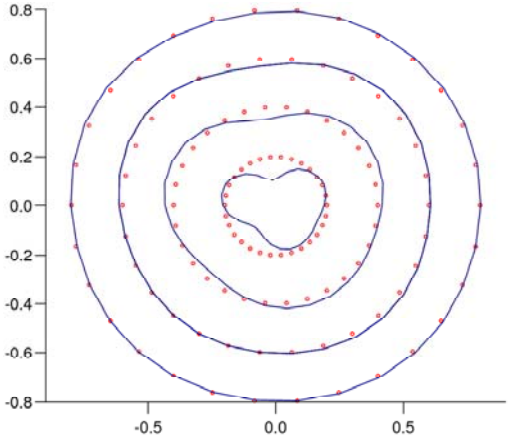

Figure 4b: The output of the regularised minimisation routine for Example 1 with $\lambda_1 = 0.05$ after the final iteration when searching for circular cavities of radii $r \in \{0.2, 0.4, 0.6, 0.8\}$ for 5% noise. The dots represent the analytical targets whilst the continuous lines represent the numerical values retrieved.

solving the inverse problem for a circular cavity provides confidence for considering examples for cavities with more complex geometries.

4.2. Example 2. In this subsection we aim to locate cavities with more complicated geometries, such as the bean shaped geometry given by the parametrisation

$$(x(\theta), y(\theta)) = \frac{0.5 + 0.4\cos\theta + 0.1\sin 2\theta}{1 + 0.7\cos\theta}(\cos\theta, \sin\theta), \quad \theta \in (0, 2\pi] \tag{25}$$

within the domain $\Omega = B_2(0, 1)$, namely Example 2.

Once again the initial guess is a circular cavity of radius 0.5 located at the origin. Unlike the previous case, see example 1, a non-analytical example is taken to specify the boundary conditions (3) and (4) as $u = 0$ on ∂D and $u = x$ on $\partial\Omega$. Since the required Neumann boundary data $\partial_n u|_{\partial\Omega}$ is not found analytically, the forward MFS procedure was implemented to calculate these values, as described in [Borman et al. 2007]. When using the data $g = \partial_n U|_{\partial\Omega}$ from the direct solver, noise was added to this data and a different M in the inverse procedure was used in order to avoid committing the inverse crime [Colton and Kress 1998]. A wide range of regularisation parameters λ_1 and λ_2 between 0 and 10^{-4} and $\lambda_3 = 0$ were investigated. When either $\lambda_1 = 0$ or $\lambda_2 = 0$, a stable result could not be achieved. An observational approach based on trial and error found that the most reliable result was achieved when $\lambda_1 = 0.07$ and $\lambda_2 = 0.05$. As expected, the results become more sensitive to selecting λ_1 and λ_2 around these values as the amount of noise increases. Numerical results are presented for $M = N_1 = 30$. Figure 5 shows the results obtained in this case when 0, 1% and 5% noise are used. It can be observed that the results are encouraging as for all noise levels a reasonable approximation to the bean shape is located. Further, the results are as accurate as the numerical results obtained by [Ivanyshyn and Kress 2006] using a boundary integral equation approach.

4.3. Example 3. We now consider a three-dimensional example which requires locating an unknown spherical cavity $D = B_3(0, r_0)$ of radius $r_0 \in (0, 1)$ within a unit sphere $\Omega = B_3(0, 1)$. We take $f = 1 - \frac{1}{r_0}$ on $\partial\Omega$ in (4), and then the direct problem given by equations (2)-(4),

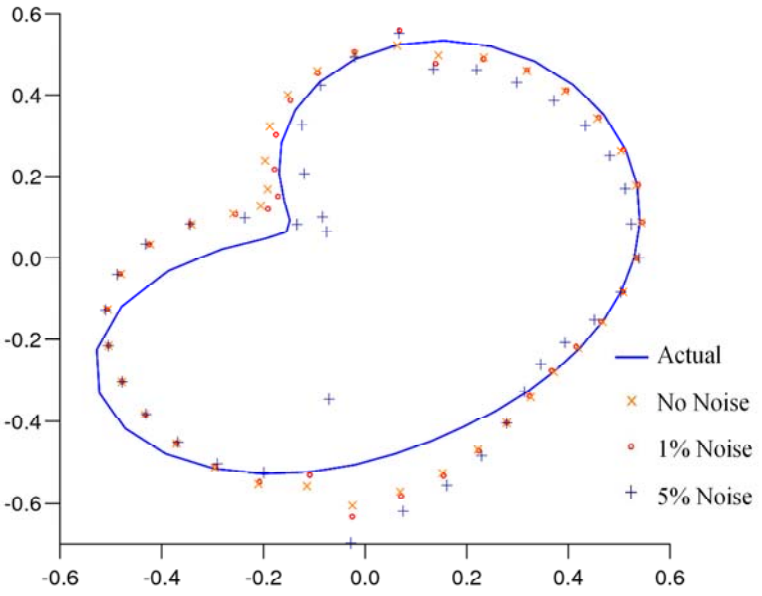

Figure 5: The output of the regularised minimisation routine for Example 2 with $\lambda_1 = 0.07$ and $\lambda_2 = 0.05$ after the final iteration when searching for a bean shaped cavity given by equation (25). The continuous line represents the analytical target whilst the points represent the numerical values retrieved for no noise, 1% and 5% noise.

when $D = B_3(0, r_0)$ is known, has the unique solution

$$u(r, \psi, \theta) = \frac{1}{r} - \frac{1}{r_0}, \qquad r_0 \leq 1 \leq 1, \qquad 0 < \psi \leq \pi, \qquad 0 < \theta \leq 2\pi. \tag{26}$$

In three-dimensions, the spherical parametrisation (9) is used for the unknown cavity D. The initial guess is taken as a sphere located at the origin with radius 0.5. This is typical for problems of this structure where a cavity is being located in the unit sphere. Numerical results are presented for $R_{ext} = s = 2$ and $M = N = 64$.

The cavity to be identified was a sphere of radius $r_0 = 0.7$ centred at the origin. Consider first the case when there is no noise added to the measured data (5) given by $g \equiv -1$ on $\partial\Omega$. Figure 6(a) shows the results obtained from the minimisation routine following a series of 800 iterations.

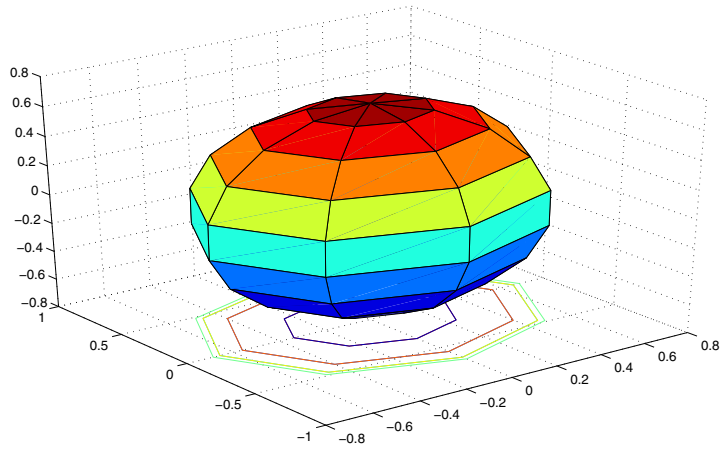

Figure 6a: The output from the minimisation routine after the final iteration for Example 3 when searching for a spherical cavity located at the origin of radius $r_0 = 0.7$ with the addition of: no noise.

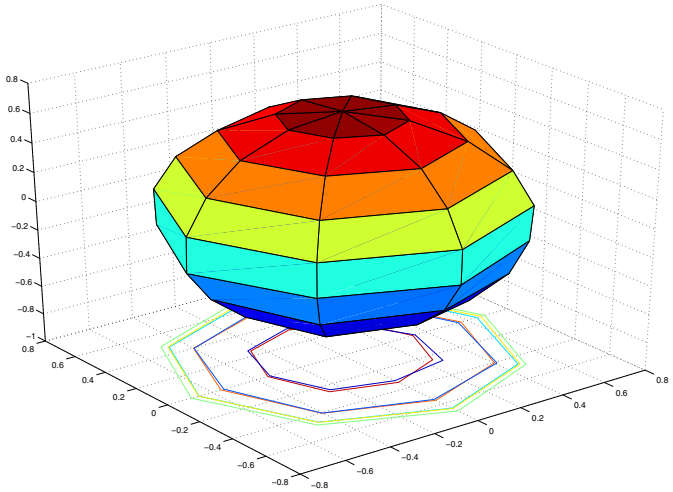

Figure 6b: The output from the minimisation routine after the final iteration for Example 3 when searching for a spherical cavity located at the origin of radius $r_0 = 0.7$ with the addition of: 2% noise.

It can be clearly seen that the routine locates the spherical cavity

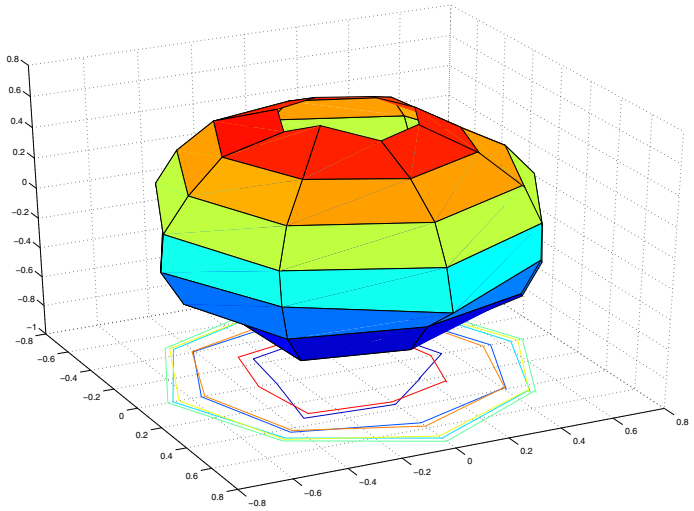

Figure 6c: The output from the minimisation routine after the final iteration for Example 3 when searching for a spherical cavity located at the origin of radius $r_0 = 0.7$ with the addition of: 5% noise.

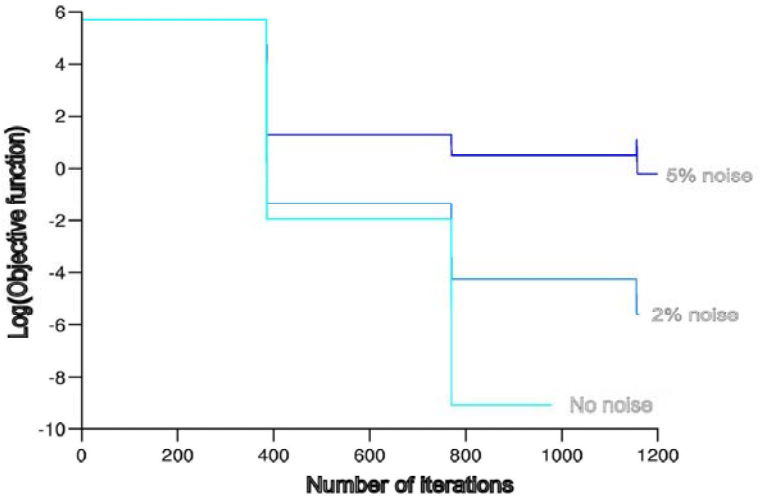

Figure 6d: The logarithm of the objective function (23), as function of the number of iterations, for Example 3 when searching for a spherical cavity located at the origin of radius $r_0 = 0.7$ with the addition of no noise, 2% and 5% noise.

of radius 0.7 with a high accuracy. Figure 6(d) shows the objective function (13) as a function of the number of iterations. From this figure it can be seen that for the first 380 iterations the solution remains almost at the initial guess after which it drops close to zero. With further sets of 380 iterations the objective function drops increasingly close to zero.

A meaningless result is obtained from the results of the minimisation routine when 2% noise is included in the measured data (5) and no regularisation is used, i.e. $\lambda_i = 0,\ i = 1, 2, 3$, in (24). This illustrates the ill-posedness of the inverse problem. Figures 6(b) and (c) show the results obtained when the regularisation parameters $\lambda_1 = \lambda_2 = 0.1$ and $\lambda_3 = 0$ are used for 2% and 5% noise, respectively. It can be observed that the numerical results demonstrate high accuracy and stability with the spherical cavity being clearly located. In figure 6(d) the minimisation of the objective function can clearly be observed for both 2% and 5% noise.

5. Conclusions. It has been shown that the MFS is well-suited for the solution of inverse cavity problems arising in EIT. The numerical experiments exhibited very accurate results for exact data, but inaccurate results when noise was introduced if no regularisation was employed. The addition of a regularisation parameter was very successful and enabled cavities to be found in a stable way for 1-5% noise added into the Neumann boundary data. As might be expected intuitively, the larger cavities were located to higher accuracies in examples containing noise. Multiple star-shaped cavities can also be located in principle by applying the MFS to each cavity as described in Section 3. The MFS technique described in this paper can be extended to solving numerically the inverse cavity problem in the acoustic field [Erhard and Potthast, 2003], the inverse acoustic scattering problem [Colton and Kress 1998, Johansson and Sleeman 2007] and the inverse electromagnetic scattering problem [Angell et al. 2003], but these investigations are deferred to a future work.

Acknowledgments. Dr D. Borman would like to acknowledge the financial support for this work from the Rothschild scheme and the University of Leeds. The comments and suggestions made by the referees are gratefully acknowledged.

REFERENCES

1. G. Alessandrini and L. Rondi, *Optimal stability estimates for the inverse problem of multiple cavities*, J. Diff. Equations, **176** (2001), 356–386.

2. C. J. S. Alves and N. F. M. Martins, *The direct method of fundamental solutions and the inverse Kirsch-Kress method for the reconstruction of elastic inclusions or cavities*, J. Integral Equations Appl., **21** (2009), 153–178.

3. ———, *The method of fundamental solutions applied to a heat conduction inverse problem*, in III European Conference on Computational Mechanics, Solids, Structures and Coupled Problems in Engineering, (eds. C. A. Mota Soares et al.), Lisbon, Portugal, 5-8 June (2006), 1–14.

4. T. S. Angell, G. C. Hsiao and L. Wen, *On the two-dimensional inverse scattering problems in electromagnetics*, Applicable Anal., **82** (2003), 483–497.

5. K. Balakrishnan and P. A. Ramachandran, *The method of fundamental solutions for linear diffusion-reaction equations*, Math. Comput. Modelling, **31** (2000) 221–237.

6. A. Bogomolny, *Fundamental solutions method for elliptic boundary value problems*, SIAM J. Numer. Anal., **22** (1985), 644–669.

7. D. Barber and B. Brown, *Applied tomography*, J. of Phys. E:Sci. Instrum., **17** (1984), 723–733.

8. K. Boone, *Introduction to Electrical Impedance Tomography, www.EIT.org.uk*, Department of Clinical Neurophysiology, Middlesex Hospital, (2006).

9. L. Borcea, *Electrical impedance tomography*, Inverse Problems, **18** (2002), R99–R136.

10. D. Borman, D. B. Ingham, T. Johansson, and D. Lesnic, *The method of fundamental solutions for direct cavity problems in EIT*, in Advances in Boundary Integral Methods - Proceedings of the Sixth UK Conference on Boundary Integral Methods, (ed. J. Trevelyan), Ch. **21** (2007), 193–202.

11. G. Burgess and E. Mahajerin, *A comparison of the boundary element method and superposition methods*, Comput. Struct. **19** (1984), 697–705.

12. D. Colton and R. Kress, *Using fundamental solutions in inverse scattering*, Inverse Problems, **22** (2006), R49–R66.

13. ———, *Inverse Acoustic and Electromagnetic Scattering Theory*, 2nd edn., Springer-Verlag, Berlin, (1998).

14. R. Duraiswami, G. L. Chahine and K. Sarkar, *Boundary element techniques for efficient 2-D and 3-D electrical impedance tomography*, Chem. Eng. Sci., **13** (1997), 2185–2196.

15. K. Erhard and R. Potthast, *The point source method for reconstructing an inclusion from boundary measurements in electrical impedance tomography and acoustic scattering*, Inverse Problems, **19** (2003), 1139–1157.

16. G. Fairweather and A. Karageorghis, *The method of fundamental solution for elliptic boundary value problems*, Adv. Comput. Math., **9** (1998), 69–95.

17. M. A. Golberg and C. S. Chen, *The method of fundamental solutions for potential, Helmholtz and diffusion problems*, in Boundary Integral Methods: Numerical and Mathematical Aspects, (ed. M. A. Goldberg), Comput. Mech. Publ., Southampton, (1998), 103–176.

18. H. Haddar and R. Kress, *Conformal mappings and inverse boundary value problems*, Inverse Problems, **21** (2005), 935–953.

19. M. Hanke and M. Bruhl, *Recent progress in electrical impedance tomography*, Inverse Problems, **19** (2003), S65–S90.

20. D. Holder, *Electrical Impedance Tomography: Methods, History and Applications*, Institute of Physics, Bristol, (2005).

21. O. Ivanyshyn and R. Kress, *Nonlinear integral equations for solving inverse boundary value problems for inclusions and cracks*, J. Integral Equations Appl., **18** (2006), 13–38.

22. T. Johansson and B. D. Sleeman, *Reconstruction of an acoustically sound-soft obstacle from one incident field and the far-field pattern*, IMA J. Appl. Math., **72** (2007), 96–112.

23. R. L. Johnston and G. Fairweather, *The method of fundamental solutions for problems in potential flow*, Appl. Math. Modelling, **8** (1982), 265–270.

24. S. Kim, O. Kwon and J. K. Seo, *Location search techniques for a grounded conductor*, SIAM J. Appl. Math., **62** (2002), 1283–1293.

25. A. Kirsch and R. Kress, *On an integral equation of the first kind in inverse acoustic scattering*, Int. Ser. Numer. Math., **77** (1986), 93–102.

26. ———, *An optimization method in inverse acoustic scattering*, in Boundary Elements IX, (eds. C.A. Brebbia, W.L. Wendland and G. Kuhn), Vol. **3**, Fluid Flow and Potential Applications, Springer-Verlag, Berlin, (1987), 3–18.

27. R. Kress, *Inverse Dirichlet problem and conformal mapping*, Math. Comput. Simulation, **66** (2004), 255–265.

28. N. F. M. Martins and A. L. Silvestre, *An iterative MFS approach for the detection of immersed obstacles*, Eng. Anal. Boundary Elements, **32** (2008), 517–524.

29. P. Serranho, *A hybrid method for inverse scattering for sound-soft obstacles in* R^3, Inverse Problems and Imaging, **1** (2007), 691–712.

30. J. R. Smith, *Field mice: extracting hand geometry from electrical field measurements*, IBM Systems J., **35** (1996), 587–608.

31. J. R. Smith, T. White, C. Dodge, J. Paradiso, N. Gershenfeld, and D. Allpost, *Electric field sensing for graphical interfaces*, IEEE Computer Graphics Appl., **18** (1998), 54–60.

Centre for Computational Fluid Dynamics, University of Leeds, Leeds LS2 9JT, UK
Email address: d.j.borman@leeds.ac.uk

Centre for Computational Fluid Dynamics, University of Leeds, Leeds LS2 9JT, UK
Email address: d.b.ingham@leeds.ac.uk

School of Mathematics, University of Birmingham, Birmingham B15 2TT, UK
Email address: b.t.johansson@bham.ac.uk

Department of Applied Mathematics, University of Leeds, Leeds LS2 9JT, UK.
Email address: amt5ld@maths.leeds.ac.uk